



Universidade de São Paulo

Biblioteca Digital da Produção Intelectual - BDPI

Departamento de Física e Ciências Materiais - IFSC/FCM

Artigos e Materiais de Revistas Científicas - IFSC/FCM

2012-10

Effect of dimensionality and morphology on polarized photoluminescence in quantum dot-chain structures

Journal of Applied Physics, College Park : American Institute of Physics - AIP, v. 112, n. 8, p. 084314-1-084314-7, Oct. 2012

<http://www.producao.usp.br/handle/BDPI/49533>

Downloaded from: Biblioteca Digital da Produção Intelectual - BDPI, Universidade de São Paulo

Effect of dimensionality and morphology on polarized photoluminescence in quantum dot-chain structures

Yu. I. Mazur, V. G. Dorogan, M. E. Ware, E. Marega, P. M. Lytvyn et al.

Citation: *J. Appl. Phys.* **112**, 084314 (2012); doi: 10.1063/1.4759318

View online: <http://dx.doi.org/10.1063/1.4759318>

View Table of Contents: <http://jap.aip.org/resource/1/JAPIAU/v112/i8>

Published by the [American Institute of Physics](#).

Related Articles

Single photon emission from impurity centers in AlGaAs epilayers on Ge and Si substrates
Appl. Phys. Lett. **101**, 172105 (2012)

A full free spectral range tuning of p-i-n doped gallium nitride microdisk cavity
Appl. Phys. Lett. **101**, 161105 (2012)

Rare earth luminescence: A way to overcome concentration quenching
AIP Advances **2**, 042115 (2012)

Two-dimensional distributed-feedback in InGaAs/GaAs quantum structure lattice arrays
Appl. Phys. Lett. **101**, 141127 (2012)

High electron mobility through the edge states in random networks of c-axis oriented wedge-shaped GaN nanowalls grown by molecular beam epitaxy
Appl. Phys. Lett. **101**, 132109 (2012)

Additional information on J. Appl. Phys.

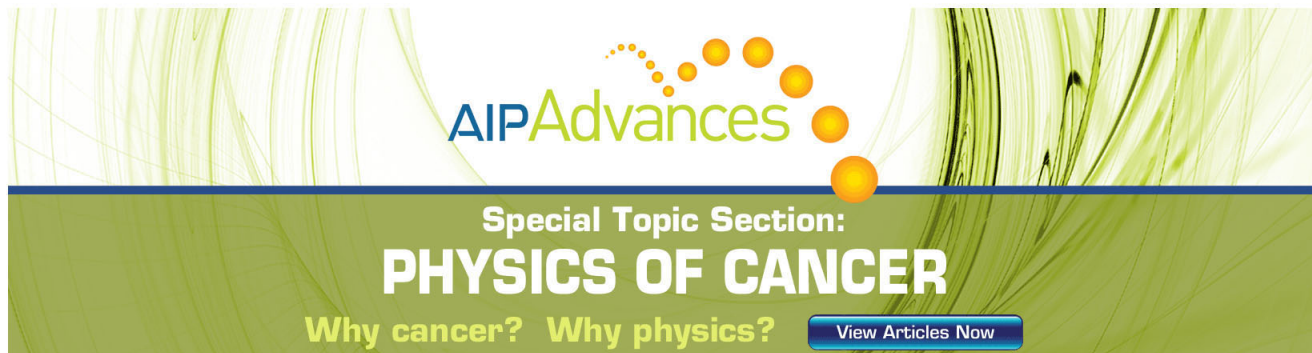
Journal Homepage: <http://jap.aip.org/>

Journal Information: http://jap.aip.org/about/about_the_journal

Top downloads: http://jap.aip.org/features/most_downloaded

Information for Authors: <http://jap.aip.org/authors>

ADVERTISEMENT



AIP Advances

Special Topic Section:
PHYSICS OF CANCER

Why cancer? Why physics? [View Articles Now](#)

Effect of dimensionality and morphology on polarized photoluminescence in quantum dot-chain structures

Yu. I. Mazur,^{1,a)} V. G. Dorogan,¹ M. E. Ware,¹ E. Marega, Jr.,^{1,b)} P. M. Lytvyn,²
Z. Ya. Zhuchenko,² G. G. Tarasov,² and G. J. Salamo¹

¹*Department of Physics, University of Arkansas, 226 Physics Building, Fayetteville, Arkansas 72701, USA*

²*Institute of Semiconductor Physics, National Academy of Sciences of Ukraine, pr. Nauki 45, Kyiv 03028, Ukraine*

(Received 12 December 2011; accepted 25 September 2012; published online 19 October 2012)

Change of the photoluminescence (PL) polarization is studied by changing the excitation intensity and temperature for aligned In(Ga)As quantum dot (QD) structures with varying inter-dot distances grown by molecular beam epitaxy on semi-insulating GaAs (100) substrates. An unusual increase of the polarization ratio is observed by increasing the temperature and/or excitation intensity throughout a low temperature ($T < 70$ K) and low intensity ($I_{\text{ex}} < 1$ W/cm²) range. This increase as well as the general behavior of the polarized PL are the results of the exciton dynamics and the peculiarities of the system morphology. They are due to the varying inter-dot distances which change the system from zero-dimensional comprised of isolated QDs to one-dimensional comprised of wire-like structures. © 2012 American Institute of Physics.

[<http://dx.doi.org/10.1063/1.4759318>]

I. INTRODUCTION

Semiconductor structures of reduced dimensionality such as quantum wells (QWs), quantum dots (QDs), quantum wires (QWRs), as well as nanorods, nanopillars, nanotubes, etc. have been the focus of both fundamental research and practical application development for several decades. Increasing the degree of quantum confinement generally leads to enhanced properties. For example, in zero-dimensional (0D) QDs, studies have found: long dephasing time and spin lifetimes, predictable sources of single-photons, strong exciton–photon coupling, and low threshold lasing.^{1,2} One-dimensional (1D), QWR structures have also demonstrated enhanced properties such as higher electron mobility, reduced nonradiative recombination, and lower threshold lasing which makes them suitable to drive the development of new devices such as nanowire solar cells,³ infrared photodetectors,⁴ nanowire injection lasers, and field-effect transistors.^{5,6} Recently, highly versatile structures have been demonstrated which exploit these systems of low dimensionality both together and separately. A QD-molecule system has been demonstrated in which the dots are tunnel coupled via connected QWRs.⁷ The more efficient tunnel coupling in this integrated QD-QWR system results in a hybridization of both electron and hole states, yielding direct-real-space excitonic molecules. Another GaAs/AlGaAs QWR-QD semiconductor system has been realized by metal organic vapor-phase epitaxy of site-controlled, self-assembled nanostructures in inverted tetrahedral pyramids.⁸ By systematically changing the length of the quantum wires, a continuous transition between the QD regime and the QWR regime can be realized. In addition to

the QD-QWR coupling, interesting physical effects have been predicted in strained segmented nanowires involving different combinations of binary compounds considered as a function of segment length.⁹ Here, wires which could demonstrate spontaneous charge separation and wires which would preferentially generate polarized exciton gases were identified. As compared with a single layer of QDs, vertically stacked QDs exhibit quasi-one-dimensional, wire-like behavior induced by vertical electronic coupling which is controlled by changing the spacer thickness.^{10,11} A transformation of the polarization of the emission from TE to TM by increasing the number of layers and increasing the vertical coupling was found and attributed to the evolution of the system from predominantly 0D into predominantly 1D structures.

Recently, laterally aligned QDs were found to create long dot-chain structures with^{12,13} and without vertical coupling.^{14–16} These (In, Ga)As/GaAs quantum dot-chain structures consist of elongated QDs aligned along the chain direction. The distances between neighboring QDs and their sizes are easily controlled by growth conditions, such that at very large dot to dot separations the ensemble acts like a collection of separate 0D QDs, and at very small separations where the dots are nearly touching, it acts more like a collection of coherent 1D nanostructures. Evidence for this 0D to 1D transition can be found in polarization-resolved photoluminescence (PL) spectroscopy, where strong linearly polarized emission along the chain direction will accompany the appearance of 1D structures. In other words, it is possible to transform the localized states of the QD exciton into propagating states of a 1D exciton in QWRs. In this paper, we investigate the PL polarization change in (In,Ga)As/GaAs quantum dot-chain structures with different inter-dot distances by varying temperature and excitation density. Such investigations allow for the distinguishing of the various mechanisms which cause linear polarization of the PL and

^{a)}Electronic address: ymazur@uark.edu.

^{b)}On leave from Departamento de Física e Ciência dos Materiais, Instituto de Física de São Carlos, USP, São Carlos SP 13560-970, Brazil.

assigning them to specifics of exciton dynamics and structural morphology.

II. SAMPLES AND EXPERIMENTAL DETAILS

The (In,Ga)As/GaAs quantum dot-chain samples were grown by molecular beam epitaxy (MBE) on semi-insulating GaAs (100) substrates consisting of 15 periods of (In_xGa_{1-x}As QD layer/60 monolayer (ML) GaAs spacer). For the QD layers, In_xGa_{1-x}As films of thicknesses 5.7, 8.5, and 15.5 MLs for x equal to 0.5 (sample C1), 0.4 (sample C2), and 0.3 (sample C3), respectively, were deposited at a temperature of 540 °C.¹⁴ This guarantees ~25% excess above the critical thickness for 2D to 3D transition for each composition as determined by *in situ* reflection high-energy electron diffraction. All samples were terminated with a final layer of uncapped QDs grown with the same composition and coverage as the underlying layers to examine the configuration by atomic force microscopy (AFM). Each of these three samples represents a different interdot coupling regime within the chains. Sample C1 ($x=0.5$) contains QDs which are significantly smaller than the interdot distances (weak coupling regime). Sample C2 ($x=0.4$) contains QDs which are only slightly smaller than their spacing (intermediate coupling regime). And, sample C3 ($x=0.3$) contains QWR structures where the QDs within a chain have merged (strong coupling regime). Topographic, AFM images of these samples are shown in Fig. 1. Associated with each image is a two-dimensional, fast Fourier transform (FFT) of a large scale (3 μm × 3 μm) AFM image of each sample. The FFTs clearly illustrate the evolution of ordering from the QDs to QWRs as the composition changes from $x=0.5$ to $x=0.3$. The wide, asymmetric QWR lobes in the FFT (Fig. 1(a)) transform into sharp features (Fig. 1(c)) testifying to the ordering of the chains/wires in the [0-11] crystallographic direction. Figure 1 reveals long QD chains laterally separated from each other by ~100 nm. At the same time, the average distance between the centers of QDs in the [0-11] crystallographic direction decreases from 65 nm in sample C1 to 44 nm in sample C2. The QD sizes in sample C1 are larger than those in sample C2 and depend on the In_xGa_{1-x}As layer thickness and composition x . Typically, the QD shape is slightly elongated along the chain direction of [0-11].^{12,13} Such unique growth morphologies are mediated by the asymmetric surface diffusivities on the GaAs (001) surface. The multilayered growth produces well-ordered QD chains where the spacing between dots and between chains can be controlled by changing the specific growth conditions.¹⁴

PL measurements were carried out at variable temperature and excitation intensity in order to better understand the effect of dimensionality and morphology on the optical properties of dot-chain structures. Excitation was with the 532 nm line of a frequency doubled Nd:YAG laser, focused to a diameter of ~30 μm at the sample. It is assumed in all that follows that using this high energy deep in-band, excitation leaves no polarization memory of the excitation in the emissions. The samples were mounted in a variable temperature 8–300 K closed-cycle helium cryostat, and the PL signal from the sample was dispersed by a monochromator and

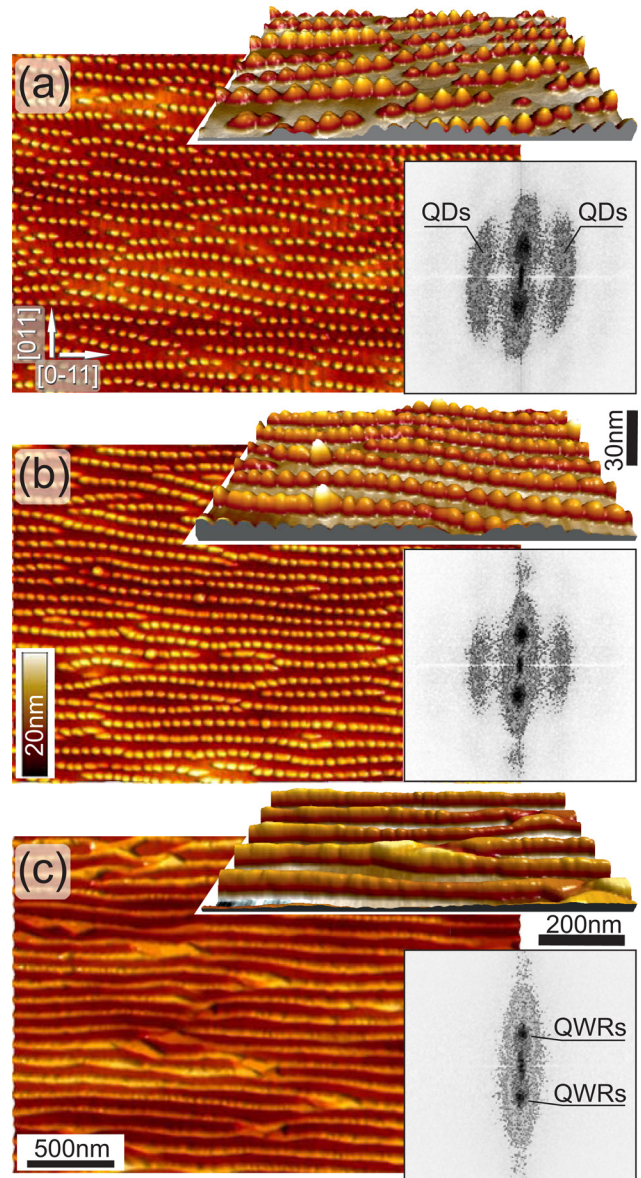


FIG. 1. AFM topographical images of samples C1, C2, and C3 [(a)–(c)]. Insets show 3D projections of sections of the corresponding surfaces and 2D Fourier transforms from a larger area (3 × 3 μm). QDs and QWRs correspond to the FFT maxima caused by regularly positioned in-chain dots (~62 nm) and wires (~87 nm).

detected by a liquid nitrogen cooled OMAV: InGaAs photodiode detector array. In order to eliminate the effect of polarization dependence of the optics and spectrometer, a quartz depolarizer was inserted along the optical axis immediately following the analyzer during polarized PL measurements.

III. EXPERIMENTAL RESULTS AND DISCUSSIONS

Figure 2 shows the PL spectra from our samples measured at low temperature and low excitation intensity ($I_{\text{ex}} = 4 \times 10^{-4} I_0$, $I_0 = 1000 \text{ W/cm}^2$), for two orthogonal polarizations: parallel to the chain direction ([0-11]) and orthogonal to it (parallel to [011]). We introduce here, the linear polarization degree, $P = (I_{0-11} - I_{011}) / (I_{0-11} + I_{011})$, with I_{0-11} and I_{011} being the intensities of the luminescence

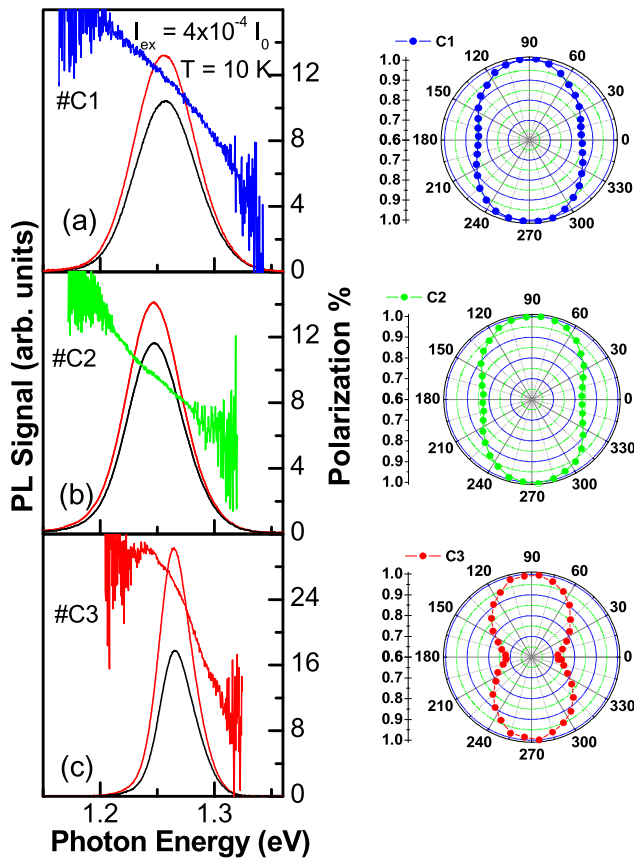


FIG. 2. Low temperature PL spectra measured in two orthogonal polarizations parallel to the [0-11] direction (red curves) and perpendicular to it ([011] direction; black curves), at low excitation intensity ($I_{ex} = 4 \times 10^{-4} I_0$, $I_0 = 1000$ W/cm²) in sample C1 (a), sample C2 (b), and sample C3 (c). Linear polarization degree $P = (I_{0-11} - I_{011}) / (I_{0-11} + I_{011})$ refers to the right ordinate axis. A polar plot of the polarized emission is shown to the right of the PL spectrum in each sample. Here, 90° corresponds to the [01-1] direction.

polarized along the [0-11] and [011] directions, respectively. In all cases, the excitation is polarized in the [0-11] direction. The spectral dependence of P for each sample is also plotted in Fig. 2 along with polar plots showing the variation of PL intensity with polarization direction. These plots clearly demonstrate the twofold symmetry of the emission. Fitting each spectra to a Gaussian reveals the peak energies and linewidths of $E_{max}^1 = 1.257$ eV and $\Gamma_1 = 64$ meV for sample C1, $E_{max}^2 = 1.247$ eV and $\Gamma_2 = 58.6$ meV for sample C2, and $E_{max}^3 = 1.266$ eV and $\Gamma_3 = 35.8$ meV for sample C3. It is well understood that QD ensemble PL linewidth is directly related to the size distribution of the QDs. Therefore, the linewidth narrowing indicates that increasing the interdot coupling strength and forming 1D structures reduce the inhomogeneous size distribution of QDs in our samples.

We find for the maximum of the PL band that the linear polarization degrees are $P_1 = 11.9\%$, $P_2 = 9.7\%$, and $P_3 = 25.9\%$ for samples C1, C2, and C3, respectively. The existence of a significant in-plane linear polarization in samples C1 and C2 is a confirmation of the anisotropy in the dot growth.¹⁷ The largest polarization is found in the wire-like sample C3, which is expected for 1D structures.¹⁸

We will now demonstrate how the observed polarization properties of asymmetric QDs are caused by the microscopic

details of the strain, valence-band mixing, and the change in the effective masses due to the strain. Using a multiband ($k \cdot p$) method, it can be shown that the anisotropic strain and quantum confinement split the degeneracy in the valence band at the Γ point into light hole (lh), heavy hole (hh), and spin-orbit (so) bands which possess different polarization properties.^{19,20} In general, the lowest confined state, which is the closest to bulk-like, is polarized along the direction of least confinement, i.e., in our case, the direction of elongation of the QDs and thus the direction of the chains or wires. Another source of the in-plane anisotropy can be piezoelectric effects.²¹⁻²⁶ These effects in zinc-blende structures arise due to the violation of inversion symmetry. In QDs, this symmetry breaking results in the appearance of piezoelectric fields along all three directions. The strength of these fields is determined by the local shear strain distribution, and as shown in Ref. 21 for InAs/GaAs QDs, the piezoelectric fields are mainly located outside of the QDs close to the QD edges. The influence of these piezoelectric fields increases with the QD sizes. Therefore, the polarization degree is expected to be higher in sample C1, than that in sample C2 because the QDs in sample C1 are larger than the QDs in sample C2 according to the results of the AFM analysis. Indeed, we do find that $P_1 > P_2$. The highest polarization degree, however, $P_3 = 25.9\%$, for this series of samples is observed in the wire-like sample C3 due to the 1D character of its excitonic states.

The linear polarization degree P is also found to be energy dependent, $P(E)$, within the spectral range of a PL band as can be seen from Fig. 2. It gradually grows from 6.8% at the high energy tail of the PL band to 13.9% at the low-energy tail in sample C1, from 6.6% to 14% in sample C2 and from 13.2% to 30% in sample C3. This is understood for the QD samples C1 and C2 as being due to the above mentioned growth of inhomogeneous strain and the strength of piezoelectric fields around larger QDs. This substantially lowers the local QD symmetry, increases the valence band mixing, and hence, increases the polarization anisotropy. Therefore, since we expect larger (more elongated) QDs to contribute to the PL band on the low energy side, we would expect the polarization to increase here too.

In the wire-like sample C3, the polarization degree reaches a maximum of $P_3 = 25.9\%$. In order to understand the nature of the polarization anisotropy in a QWR system, many sources have to be taken into account. There exists two basic sources of anisotropy for the optical transitions in a QWR: (i) a strong valence band mixing (due to spatial confinement and strain)²⁷⁻³³ and (ii) a discontinuity in the dielectric constant between the wire and its surroundings (due to optical confinement).³⁴⁻³⁹ It is shown within the framework of a $k \cdot p$ approximation that the maximum degree of linear polarization produced by mixing the bulk Γ_8 states is $\sim 60\%$ for the ground state $h1-e1$ transition, independent of wire orientation, diameter, or composition.^{27,30} The optical confinement caused by the difference in dielectric constants, ϵ , for QWRs and their surroundings, e.g., $\epsilon = 14.6$ for an InAs semiconductor wire versus $\epsilon = 1$ for air, leads to even higher P values. For isolated GaN nanorods³⁹ or InP nanowires,³⁶ size dependent polarization anisotropy was observed above 90%.

Taking into account that the QWRs in sample C3 are sufficiently wide (~ 100 nm), we can expect polarization contributions from both valence band mixing and dielectric discontinuities. Indeed, valence band mixing is essential in comparatively thin QWRs. For thin (several tens of nm) $\text{In}_x\text{Ga}_{1-x}\text{As}/\text{GaAs}$ wires, the extension of the exciton wave function (double Bohr radius $2a_B \approx 26$ nm) becomes comparable to the wire width and pronounced confinement effects are expected to develop. If the wire width significantly exceeds this Bohr radius, the quantization energy decreases and will approach the thermal energy or the level broadening, where the size quantization is no longer observable. Here, polarization due to the discontinuity in the dielectric constant can dominate. In order to estimate the contribution of optical confinement to P in sample C3, we can use the dipole approximation for the luminescence strength which is proportional to the scalar product of the local electric field \vec{E} and the inter-band dipole moment, \vec{d} , averaged over the full electron-hole wave function. Then one gets^{33,35}

$$P = \frac{|d_{cv}^{\parallel}|^2 - \delta^2 |d_{cv}^{\perp}|^2}{|d_{cv}^{\parallel}|^2 + \delta^2 |d_{cv}^{\perp}|^2}, \quad (1)$$

where $d_{cv}^i = \langle \Psi_c | d^i | \Psi_v \rangle$ is the dipole matrix element between conduction (c) and valence (v) bands for the $i = \parallel, \perp$ components of the dipole moment parallel and perpendicular to the wire axis. In Eq. (1),

$$\delta = \frac{2\varepsilon_s}{\varepsilon_s + \varepsilon_w}, \quad (2)$$

with ε_s and ε_w being the dielectric constants of the surrounding material and the wire, respectively. We take $\varepsilon_s = 13.1$ for GaAs and $\varepsilon_w = 13.55$ for $\text{In}_{0.3}\text{Ga}_{0.7}\text{As}$, which was derived by linear extrapolation from $\varepsilon = 14.6$ for InAs, and make a simplifying approximation of $|d_{cv}^{\perp}| = |d_{cv}^{\parallel}|$, i.e., no anisotropy in the dipole moment. Then we can use Eq. (1) to estimate the contribution to P from the dielectric discontinuity alone to be equal 1.7% only. Thus, we conclude that the main contribution to P in our samples must be from the anisotropy of the dipole matrix elements in Eq. (1), which is determined by the valence band mixing. This mixing in QWRs is not only due to lateral confinement, but can also be affected by high-index confinement,⁴⁰ anisotropic strain,⁴¹ and anisotropic interface roughness.⁴² For example, it has been shown⁴¹ that for compressively strained, InAsP QWRs, large in-plane polarization anisotropy is caused by the broken symmetry due to the effective triaxial anisotropic strain alone. As a result, the net effect on the valence band mixing becomes rather complicated.

Using a first order approximation for the valence band mixing,²⁹ the optical anisotropy that results from lateral confinement and anisotropic strain can be reduced to the following simple relation:⁴³

$$\left[\frac{\gamma_2 \hbar^2 \pi^2}{m_0 l^2} + b(e_{\perp} - e_{\parallel}) \right] / (E_{hh} - E_{lh}). \quad (3)$$

Here, γ_2 is the Luttinger parameter for the hole effective mass, b is the shear deformation potential ($b > 0$), e_{\parallel} and e_{\perp} are the strain components along and perpendicular to the wire axis, and l is the lateral extent of the hole wave function which is equal to the QWR width for sufficiently wide QWRs. From Eq. (3), it follows that the optical anisotropy becomes inversely proportional to the square of the QWR width. In turn, the biaxial strain in the wires leads only to an increase of the difference, $E_{hh} - E_{lh}$, which reduces the optical anisotropy again. In the case of triaxial strain, the optical anisotropy can be enhanced, because $(e_{\perp} - e_{\parallel}) > 0$ due to strain in the normal direction. Thus, coming back to Fig. 2(c), we conclude that a large value of the polarization degree even in wide QWRs can be assigned to the lateral confinement enhanced due to the anisotropic strain in the vicinity of the QWR interfaces. Larger QWRs induce larger symmetry distortion, exhibit a significant piezoelectric field, have a larger degree of valence band mixing, and as a result increase the polarization degree. Therefore, the observed polarization in sample C3 grows as the energy decreases within the QWR PL band as shown in Fig. 2(c).

Figure 3 demonstrates the changes of the PL line-shape and polarization degree for higher intensity excitation, $I_{\text{ex}} = 5 \times I_0$. The spectra of all samples at this higher power demonstrate a significant blue shift and broadening of the ground state exciton PL band: $E_{\text{max}}^1 = 1.257 \text{ eV} \rightarrow 1.271 \text{ eV}$ and $\Gamma_1 = 64 \text{ meV} \rightarrow 100 \text{ meV}$ in sample C1, $E_{\text{max}}^2 = 1.247 \text{ eV} \rightarrow 1.272 \text{ eV}$ and $\Gamma_2 = 58.6 \text{ meV} \rightarrow 96.5 \text{ meV}$

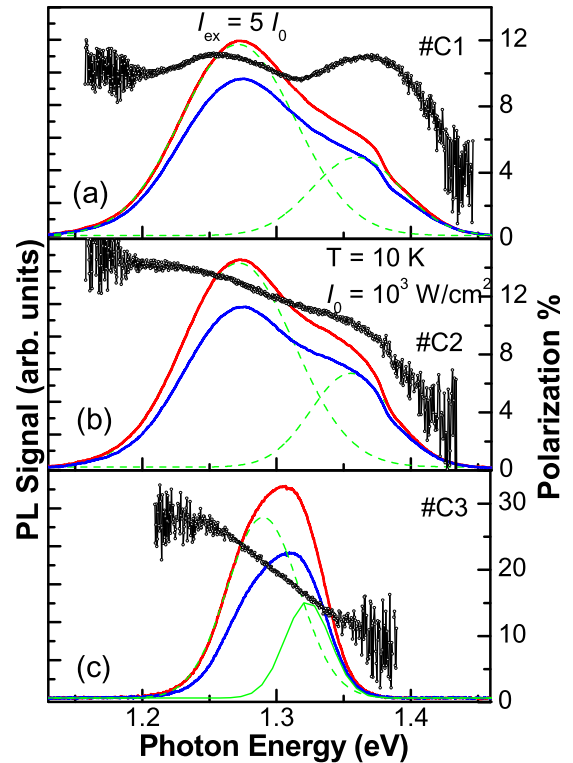


FIG. 3. Low temperature PL spectra and linear polarization degree P measured in polarizations parallel to the $[0\bar{1}1]$ direction and along the $[011]$ direction at high excitation intensity ($I_{\text{ex}} = 10 \times I_0$) in sample C1 (a), sample C2 (b), and sample C3 (c).

in sample C2, and $E_{\max}^3 = 1.266 \text{ eV} \rightarrow 1.290 \text{ eV}$ and $\Gamma_3 = 35.8 \text{ meV} \rightarrow 61 \text{ meV}$ in sample C3. In addition, a higher energy PL band develops at $E_{\max}^{1a} = 1.355 \text{ eV}$ with $\Gamma_{1a} = 77 \text{ meV}$ in sample C1, $E_{\max}^{2a} = 1.355 \text{ eV}$ with $\Gamma_{2a} = 69.5 \text{ meV}$ in sample C2, and at $E_{\max}^{3a} = 1.323$ with $\Gamma_{3a} = 40 \text{ meV}$ in sample C3. The blue shift and broadening of the PL bands are attributed to the state filling effect that results in the appearance of the excited QD states. At high excitation intensity, such as in Fig. 3, we believe that the piezoelectric fields are fully screened by the photo-excited carriers both in the QD and QWR samples.

The higher energy peak for the QD samples, C1 and C2, has been assigned to a one-dimensional wetting layer (1D WL) state,^{12,44,45} in analogy to the 2D WL generally arising during Stranski-Krastanov growth of QDs. It has been shown,⁴⁵ however, that this 1D WL develops after the dot formation, during overgrowth with GaAs creating a 1D channel between and connecting the dots in a line. As seen in Figs. 3(a) and 3(b) at the maximum of this PL band, the polarization degree reaches a comparatively high value of $P \approx 11\%$ which would be expected for 1D structures. In sample C3, however, the dots themselves form a 1D wire-like structure (see Fig. 1(c)) which, in principle, prevents the formation of a second, separate 1D WL structure. Thus, the source of the additional band in the high intensity PL spectra of sample C3 is most likely, simply an excited state of the QWR structure rather than PL from a separate 1D WL as in samples C1 and C2.

In order to gain further insight into the nature of the PL anisotropy in the wire-like sample C3, we carried out a calculation of the polarization degree as a function of the excitation intensity for rectangular InGaAs QWRs using an approach similar to that applied for strain-induced laterally ordered $\text{In}_{0.4}\text{Ga}_{0.6}\text{As}$ QWRs on GaAs (311)A.⁴⁶ Using the adjusted Hamiltonian by Bockelmann and Bastard,²⁷ we calculated the squared, transition matrix elements, $M_{ij}(k_y)$, between the conduction band state (i, k_y) and the valence band state (j, k_y) (here y is along the QWR axis). For the case of linearly polarized light propagating perpendicular to the plane of the QWRs, this results in

$$|M_{ij}(k_y)|^2 = \frac{1}{2} \left\{ |J_{ij}^{3/2}|^2 + |J_{ij}^{-3/2}|^2 \right\} + \frac{1}{6} \left\{ |J_{ij}^{1/2}|^2 + |J_{ij}^{-1/2}|^2 \right\} + \frac{1}{\sqrt{3}} \text{Re} \left\{ J_{ij}^{3/2} J_{ij}^{-1/2*} + J_{ij}^{1/2} J_{ij}^{-3/2*} \right\} \cos 2\vartheta. \quad (4)$$

Here, the overlap integrals for the electron and hole envelope functions are

$$J_{ij}^{\mu} = \int dx dz \varphi_i^{c*}(x, z) \varphi_{\mu j}^v(x, z), \quad (5)$$

where $\mu = \{3/2, 1/2, -1/2, -3/2\}$ denotes the components of the hole wave function, and ϑ is the angle between the polarization vector of light and the QWR's axis (y -direction). The QWR PL intensity is then given by

$$I(\hbar\omega) \propto (\hbar\omega)^2 \sum_{ij} \int_{-\infty}^{\infty} dk_y \int_{-\infty}^{\infty} dE_c \int_{-\infty}^{\infty} dE_v \delta(E_c - E_i^c(k_y)) \times \delta(E_v - E_j^v(k_y)) |M_{ij}(k_y)|^2 \delta(E_c - E_v - \hbar\omega) \times F(E_c - E_F^c) F(E_v - E_F^v). \quad (6)$$

Now, we have the 1D density of states in the conduction and valence band given by

$$D^{c,v}(E) = \frac{2}{\pi} \sum_l \int_{-\infty}^{\infty} dk_y \delta(E - E_l^{c,v}(k_y)), \quad (7)$$

where $E_l^{c,v}(k_y)$ are the energy dispersion branches for electrons and holes. The quasi-Fermi energies E_F^c and E_F^v of the conduction and valence bands are determined from the conditions

$$n = \int_{-\infty}^{\infty} D^c(E) F(E - E_F^c) dE = \int_{-\infty}^{\infty} D^v(E) F(E - E_F^v) dE. \quad (8)$$

A Lorentzian broadening function is used instead of the delta function, determining the energy conservation law in Eq. (7), which accounts for the uncertainty due to a finite lifetime of the electron and hole states. In order to calculate PL intensity $I(\hbar\omega)$ and the polarization degree, P , as a function of excitation density, the density of excess carriers n_{exc} and the excitation density I_0 were assumed to be proportional ($n_{exc} \propto I_{exc}$).

The results of these calculations are shown in Fig. 4 as the solid line. Here, we see both the measured and calculated polarization degrees taken at the PL maximum for sample C3 as a function of excitation intensity. It can be seen that the theoretical dependence, calculated assuming perfect rectangular QWRs and taking into account only the phase-space filling and electron-hole wave-function overlap, describes the high intensity side of the experimental data quite well. In the low intensity range, however, theory and experiment give very different results. This deviation between the

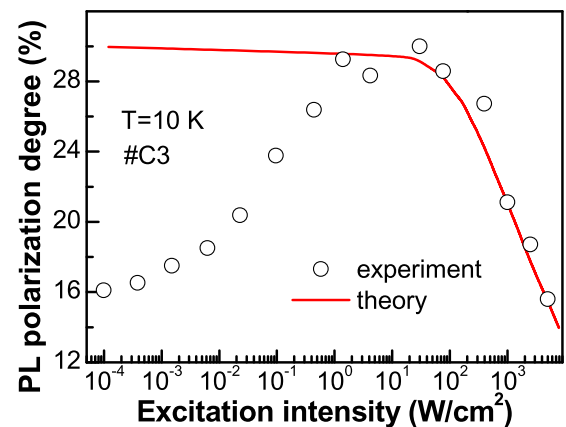


FIG. 4. Dependence of the linear polarization degree, P , on excitation intensity, I_{exc} , in the wire-like sample C3: circles—experimental results; solid line—theory.

theoretical dependence which reaches a maximum and the experimental, P , dependence which falls quickly as the excitation power is reduced to a minimum, indicates that real QWR behavior at low excitation intensities does not correlate with the behavior of a pure 1D system. We believe the localization of 1D excitons into 0D states by wire imperfections or in-plane piezoelectric fields to be the source of the non-ideal nature of the 1D QWRs. At low power excitation and low temperature, 1D excitons can be trapped by fluctuations of the local potential. This localization reduces the 1D wire to an ensemble of effective 0D QDs significantly influencing the symmetry of the excitons and hence the polarization rules for the optical transitions. As a result, the polarization degree decreases at low excitation intensities. With an increase in hot carrier concentration in the QWR region due to an increase in excitation intensity or temperature, the excitons, which dominantly contribute to the PL, are from the unbound states where they are free to move in the 1D band. The degree of polarization thus grows with the excitation intensity, and the experimental points in Fig. 4 tend to the theoretical values calculated for the ideal 1D structure. Further increase in intensity begins to screen the internal fields and ultimately saturates the polarization. Before the full density of states of the QWRs become filled, thus populating the WL, we believe the biexciton-like states become populated which through the anisotropic exchange mechanism are polarized perpendicularly to the ground state excitons. The emitted light, being the sum of all mechanisms, would then lose some polarization value, which is observed experimentally. These observed characteristics of the polarization degree with increasing excitation intensity correlate with the behavior of the PL decay time in this QWR structure (sample C3) observed earlier by means of time resolved spectroscopy as a function of temperature.¹⁴

A similar scenario is observed in the temperature dependences of the degree of polarization for our samples. Figure 5 shows the $P(T)$ dependences measured at the maximum of the PL band in each of samples C1, C2, and C3. The low temperature growth of $P(T)$ observed in the QD samples derives from thermally activated carrier transfer to larger QDs or QWRs that generate stronger piezoelectric fields at the interfaces. Due to stronger mixing of the valence bands caused by these stronger piezoelectric fields, the emitted light has a higher degree of polarization. Further temperature increase does not change the $P(T)$ value in sample C1, slightly reduces it in sample C2, and drastically reduces it in sample C3 at a rate of 0.13%/K within the temperature range 50–200 K. The temperature induced reduction of the $P(T)$ in comparatively wide QWRs and large QDs is attributed to effective population of the excited hole states with the increase in temperature. While the energy gap between the hole states decreases with the growth of lateral dimensions, the moderate temperature leads to a thermal population of the excited states. Emission from these states can be polarized perpendicular to the wire axis,⁴⁷ resulting in the temperature induced depolarization of the emitted light. It should be noted that similar to the power dependent results, we have a low temperature range where everything acts like a QD due to localization effects, i.e., the polarization increases as

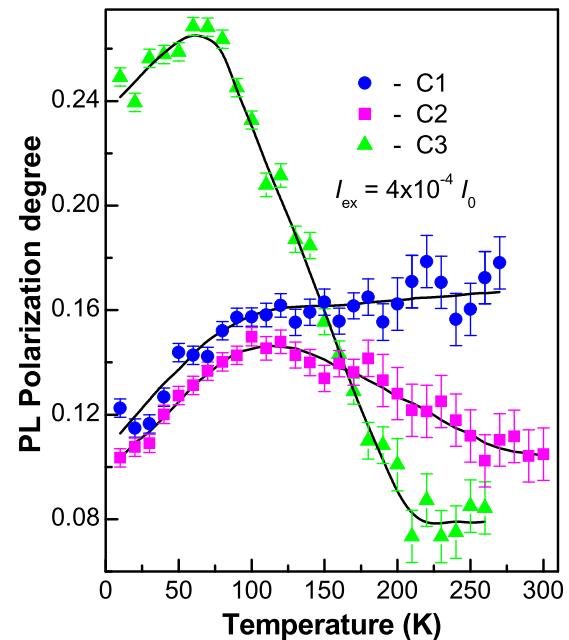


FIG. 5. Temperature dependence of the linear polarization degree, P , measured at the PL maximum with ($I_{\text{ex}} = 4 \times 10^{-4} I_0$, $I_0 = 1000 \text{ W/cm}^2$) in sample C1 (circles), sample C2 (squares), and sample C3 (triangles). Lines are guides to the eye only.

the “larger” structures are populated. However, at some point, the true QDs saturate due to the discrete nature of the energy spectrum. Finally, similar to the high excitation power case, the polarization at higher temperatures vanishes for the QWR-like structures.

IV. CONCLUSIONS

Concluding, the change of the PL polarization is studied by changing excitation intensity and temperature for aligned In(Ga)As QD structures with varying inter-dot distances grown by molecular beam epitaxy on semi-insulating GaAs (100) substrates. An unusual increase of the polarization ratio is observed with temperature and/or excitation intensity in the low temperature ($T < 70 \text{ K}$) and low intensity ($I_{\text{ex}} < 1 \text{ W/cm}^2$) ranges. This increase as well as the general behavior of the polarized PL in the structures under consideration is attributed to the exciton dynamics changing from 0D, QD-like, to 1D, wire-like and to the peculiarities of the resulting system morphologies.

ACKNOWLEDGMENTS

The authors acknowledge the financial support of the NSF (through Grant No. DMR-0520550).

¹Z. I. Alferov, *Rev. Mod. Phys.* **73**, 767 (2001).

²D. J. Mowbray and M. S. Skolnick, *J. Phys. D: Appl. Phys.* **38**, 2059 (2005).

³M. Law, L. E. Greene, J. C. Johnson, R. Saykally, and P. Yang, *Nature Mater.* **4**, 455 (2005).

⁴H. Pettersson, J. Tragardh, A. I. Persson, L. Landin, D. Hessman, and L. Samuelson, *Nano Lett.* **6**, 229 (2006).

⁵X. Duan, Y. Huang, R. Agarwal, and C. M. Lieber, *Nature* **421**, 241 (2003).

- ⁶Y. Cui, X. Duan, Y. Huang, and C. M. Lieber, "Nanowires as building blocks for nanoscale science and technology," in *Nanowires and Nanobelts: Materials, Properties and Devices*, edited by Z. L. Wang (Kluwer Academic/Plenum, 2003), pp. 3–68.
- ⁷Q. Zhu, K. F. Karlsson, M. Byszewski, A. Rudra, E. Pelucchi, Z. He, and E. Kapon, *Small* **5**, 329 (2009).
- ⁸Q. Zhu, K. F. Karlsson, E. Pelucchi, and E. Kapon, *Nano Lett.* **7**, 2227 (2007).
- ⁹M.-E. Pistol and C. E. Pryor, *Phys. Rev. B* **80**, 035316 (2009).
- ¹⁰P. Yu, W. Langbein, K. Leosson, J. M. Hvam, N. N. Ledentsov, D. Bimberg, V. M. Ustinov, A. Yu. Egorov, A. E. Zhukov, A. F. Tsatsul'nikov, and Yu. G. Musikhin, *Phys. Rev. B* **60**, 16680 (1999).
- ¹¹T. T. Chen, Y. F. Chen, J. S. Wang, Y. S. Huang, R. S. Hsiao, J. F. Chen, C. M. Lai, and J. Y. Chi, *Semicond. Sci. Technol.* **22**, 1077 (2007).
- ¹²Yu. I. Mazur, W. Q. Ma, X. Wang, Z. M. Wang, G. J. Salamo, M. Xiao, T. D. Mishima, and M. B. Johnson, *Appl. Phys. Lett.* **83**, 987 (2003).
- ¹³M. Schmidbauer, Sh. Seydmohamadi, D. Grigoriev, Zh. M. Wang, Yu. I. Mazur, P. Schäfer, M. Hanke, R. Köhler, and G. J. Salamo, *Phys. Rev. Lett.* **96**, 066108 (2006).
- ¹⁴Yu. I. Mazur, V. G. Dorogan, E. Marega, Jr., P. M. Lytvyn, Z. Ya. Zhuchenko, G. G. Tarasov, and G. J. Salamo, *New J. Phys.* **11**, 043022 (2009).
- ¹⁵Yu. I. Mazur, V. G. Dorogan, E. Marega, Jr., G. G. Tarasov, D. F. Cesar, V. Lopez-Richard, G. E. Marques, and G. J. Salamo, *Appl. Phys. Lett.* **94**, 123112 (2009).
- ¹⁶Yu. I. Mazur, V. G. Dorogan, E. Marega, Jr., D. F. Cesar, V. Lopez-Richard, G. E. Marques, Z. Ya. Zhuchenko, G. G. Tarasov, and G. J. Salamo, *Nanoscale Res. Lett.* **5**, 991 (2010).
- ¹⁷H. Saito, K. Nishi, S. Sugou, and Y. Sugimoto, *Appl. Phys. Lett.* **71**, 590 (1997).
- ¹⁸F. Vouilloz, D. Y. Oberli, M.-A. Dupertuis, A. Gustafsson, F. Reinhardt, and E. Kapon, *Phys. Rev. B* **57**, 12378 (1998).
- ¹⁹U. Woggon, *Optical Properties of Semiconductor Quantum Dots* (Springer-Verlag, Berlin, 1997).
- ²⁰D. Bimberg, M. Grundmann, and N. N. Ledentsov, *Quantum Dots Heterostructures* (Wiley, New York, 1999).
- ²¹M. Grundmann, O. Stier, and D. Bimberg, *Phys. Rev. B* **52**, 11969 (1995).
- ²²G. Pryor, *Phys. Rev. B* **57**, 7190 (1998).
- ²³O. Stier, M. Grundmann, and D. Bimberg, *Phys. Rev. B* **59**, 5688 (1999).
- ²⁴*Nano-Optoelectronics Concepts, Physics and Devices*, edited by M. Grundmann (Springer, Berlin, 2002), Chap. 7.
- ²⁵S. Hackenbuchner, M. Sabathil, J. Majewski, G. Zandler, P. Vogl, E. Beham, A. Zrenner, and P. Lugli, *Physica B* **314**, 145 (2002).
- ²⁶G. Bester and A. Zunger, *Phys. Rev. B* **71**, 045318 (2005).
- ²⁷P. C. Sercel and K. J. Vahala, *Appl. Phys. Lett.* **57**, 545 (1990).
- ²⁸P. C. Sercel and K. J. Vahala, *Phys. Rev. B* **44**, 5681 (1991).
- ²⁹U. Bockelmann and G. Bastard, *Phys. Rev. B* **45**, 1688 (1992).
- ³⁰A. A. Yamaguchi and A. Usui, *J. Appl. Phys.* **78**, 1361 (1995).
- ³¹D. S. Citrin and Y.-C. Chang, *J. Appl. Phys.* **70**, 867 (1991).
- ³²W. H. Zheng, J.-B. Xia, and K. W. Cheah, *J. Phys.: Condens. Matter* **9**, 5105 (1997).
- ³³M. Califano and A. Zunger, *Phys. Rev. B* **70**, 165317 (2004).
- ³⁴P. Ils, Ch. Greus, A. Forchel, V. D. Kulakovskii, N. A. Gippius, and S. G. Tikhodeev, *Phys. Rev. B* **51**, 4272 (1995).
- ³⁵E. A. Muljarov, E. A. Zhukov, V. S. Dneprovskii, and Y. Masumoto, *Phys. Rev. B* **62**, 7420 (2000).
- ³⁶J. Wang, M. S. Gudiksen, X. Duan, Y. Cui, and C. M. Lieber, *Science* **293**, 1455 (2001).
- ³⁷H. E. Ruda and A. Shik, *Phys. Rev. B* **72**, 115308 (2005).
- ³⁸H. E. Ruda and A. Shik, *J. Appl. Phys.* **100**, 024314 (2006).
- ³⁹H.-Y. Chen, Y.-C. Yang, H.-W. Lin, S.-C. Chang, and S. Gwo, *Opt. Express* **16**, 13465 (2008).
- ⁴⁰C.-N. Chen, *Phys. Rev. B* **72**, 085305 (2005).
- ⁴¹M. Notomi, J. Hammersberg, J. Zeman, H. Weman, M. Potemski, H. Sugiura, and T. Tamamura, *Phys. Rev. Lett.* **80**, 3125 (1998).
- ⁴²G. E. W. Bauer and H. Sakaki, *Surf. Sci.* **267**, 442 (1992).
- ⁴³J. Wu, Y. H. Chen, and Z. G. Wang, *J. Nanosci. Nanotechnol.* **8**, 3300 (2008).
- ⁴⁴X. Wang, Z. M. Wang, B. Liang, G. J. Salamo, and C. K. Shih, *Nano Lett.* **6**, 1847 (2006).
- ⁴⁵Z. M. Wang, Yu. I. Mazur, J. L. Shultz, G. J. Salamo, T. D. Mishima, and M. B. Johnson, *J. Appl. Phys.* **99**, 033705 (2006).
- ⁴⁶Yu. I. Mazur, Zh. M. Wang, G. G. Tarasov, H. Wen, V. Strelchuk, D. Guzun, M. Xiao, G. J. Salamo, T. D. Mishima, G. D. Lian, and M. B. Johnson, *J. Appl. Phys.* **98**, 053711 (2005).
- ⁴⁷T. Sogawa, H. Ando, S. Ando, and H. Kanbe, *Phys. Rev. B* **56**, 1958 (1997).